Synthesis and electrical transport properties of superconducting platinum silicide thin films and devices

T. Nanayakkara, M. Liu

To be published in "Journal of Vacuum Science & Technology A"

December 2024

DISCLAIMER

Synthesis and Electrical Transport Properties of Superconducting Platinum Silicide Thin Films and Devices

Tharanga R. Nanayakkara,[1] Anthony T. Bollinger,[2] Ruoshui Li,[1,3] Chenyu Zhou,[1] Abdul K. Rumaiz,[4] Xiao Tong,[1] Lihua Zhang,[1] Kim Kisslinger,[1] Charles T. Black,[1] and Mingzhao Liu[1]
[1]*Center for Functional Nanomaterials, Brookhaven National Laboratory, Upton, NY 11973, USA*
[2]*Condensed Matter Physics and Materials Science Division, Brookhaven National Laboratory, Upton, NY 11973, USA*
[3]*Department of Chemistry, Stony Brook University, Stony Brook, NY 11794, USA*
[4]*National Synchrotron Light Source II, Brookhaven National Laboratory, Upton, NY 11973, USA*

(*Electronic mail: mzliu@bnl.gov)

(*Electronic mail: ctblack@bnl.gov)

(Dated: 19 September 2024)

We evaluate the material characteristics of superconducting platinum silicide (PtSi) thin films as candidate materials for superconducting quantum information devices compatible with silicon technology. These films were synthesized using magnetron sputtering under ultra-high vacuum conditions, followed by rapid thermal annealing. Polycrystalline PtSi films synthesized by this method have the favorable properties of superconducting critical temperature of 0.95 K and relatively long zero-temperature Ginzburg-Landau coherence length of 76 nm. We further studied co-planar microbridge devices fabricated by electron beam lithography and chlorine-free reactive ion etching, finding that the temperature dependent critical current density follows the Ginzburg Landau de-pairing mechanism.

I. INTRODUCTION:

With the urgent rush to develop superconducting quantum information devices, a critical phase involves evaluating and selecting materials with advantageous properties, particularly in the cryogenic environments in which qubits operate.[1] For example, aluminum and niobium have been longtime materials of choice, with tantalum recently demonstrating substantial benefits.[2–4] Even with continuing performance improvements, it is vital to explore alternative superconducting materials that may offer further performance advantages. Because there is strong incentive to develop qubit fabrication processes that fit within silicon technology, our group and others have been investigating superconducting transition metal (TM) silicides. TM silicides are highly compatible with silicon processing, which offers significant advantages for scalability and development of quantum computing systems.

Among TM silicides, platinum silicide (PtSi) has found broad application in electronic devices and CMOS technologies[5,6], including source/drain contact in field effect transistors,[7] Schottky diodes,[8] infrared (IR) detectors,[9] field-effect transistor gates, and micro-electro-mechanical systems (MEMS) devices,[10] due to its high electrical conductivity and thermal/chemical stability. PtSi is also a superconductor, and has been used in microwave kinetic inductance detectors (MKIDs) and quantum phase slip junctions.[11–15]

In this work, we measure the material properties and electrical transport in superconducting PtSi thin films grown on Si(100) wafers. Measurements of the field-temperature (H-T) phase diagram and depairing critical current density of PtSi thin films determine a critical temperature close to 1 K, with zero-temperature Ginzburg-Landau coherence length of 76 nm, and Pippard coherence length of 460 nm.

II. RESULTS AND DISCUSSION

A. PtSi thin film synthesis and characterization

PtSi thin films were synthesized on silicon wafers by depositing a Pt layer using magnetron sputtering. The Pt-covered Si substrate was then subjected to rapid thermal processing, converting the Pt layer into PtSi (details in *Methods*). The average thickness of the PtSi thin film, as measured by cross-sectional scanning electron microscopy, is 25 nm (Fig. 1(a)). Atomic force microscopy of the PtSi surface reveals that the film is flat, with root-mean-squared roughness of 1.2 nm (Fig. 1(b)).

Grazing incident X-ray diffraction (GIXRD) measurements were carried out on the PtSi thin films in the ranges of diffraction angles $18^\circ \leq 2\theta \leq 70^\circ$, with the grazing incidence angle fixed at about 0.5°. The GIXRD confirms formation of PtSi in orthorhombic lattice, without trace of intermediate phases of platinum silicides, such as Pt_3Si or Pt_2Si,[16,17] confirming the complete conversion of Pt to PtSi. The peak positions corresponding to the various crystal orientations of PtSi are identified (Fig. 1(c)). Narrow peaks indicate well-ordered and crystalline nature of PtSi. The polycrystalline nature of PtSi on Si(100) is understood as a result of lattice mismatch ($\sim 10\%$) between PtSi and Si.[15,18]

To confirm the PtSi film chemical composition, we conducted scanning transmission electron microscopy (STEM) studies on vertical cross-sectional specimens, prepared with the focused ion beam (FIB) lift-out technique. The high-angle annular dark field (HAADF)-STEM image (Fig. 2a) confirms the presence of a thin, PtSi layer atop the Si wafer. The energy-dispersive X-ray spectroscopy (EDX) mapping, collected concurrently with the HAADF-STEM image, reveals

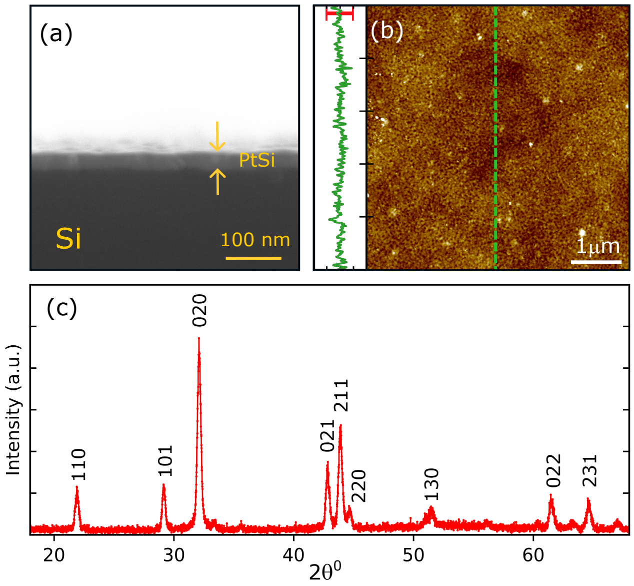

FIG. 1. (a) Cross-sectional SEM image of a 25 nm thick PtSi film synthesized on Si(100). (b) Atomic force microscope (AFM) topographical image of the PtSi surface. Side panel shows the height profile along the green dashed line. Red scale bar = 10 nm. (c) Grazing incidence X-ray diffraction (GIXRD) pattern of a PtSi thin film.

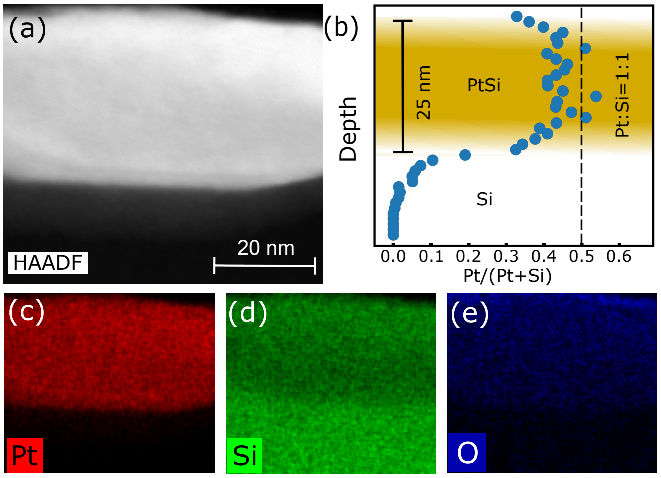

FIG. 2. (a) HAADF-STEM image of a PtSi thin film on Si(100). (b) Quantitative EDX analysis reveals nearly 1:1 Pt:Si ratio within the PtSi layer. (c), (d) and (e) EDX elemental mapping for the spatial distributions of platinum (Pt), silicon (Si) and oxygen (O) respectively, collected simultaneously with the HAADF-STEM image in panel (a).

nearly 1:1 atomic ratio between Pt and Si (Fig. 2b) and confirms the uniform distribution of Pt and Si within the PtSi layer (Fig. 2c and d).

Surface chemistry of PtSi thin films was examined by X-ray photoelectron spectroscopy (XPS), using Al K_α radiation ($h\nu$ = 1486.6 eV) as the excitation source. XPS scans collected near the edge of the 2-inch PtSi wafer (Figs. 3a and b) appear almost identical to those collected near the wafer center (Figs. 3c and d), signifying the thin film uniformity across the entire wafer. The XPS survey scans confirm the absence of impurity metal elements in the PtSi thin film. However, the O 1s peak, with its binding energy (B.E.) at approximately 530 eV, clearly indicates surface oxidation. The Pt 4f envelope displays a doublet induced by spin–orbit coupling, with the Pt $4f_{7/2}$ component peaking at 72.2 eV, affirming the intermetallic nature of Pt in PtSi (Figs. 3b and d).[19–22] Meanwhile, the Si 2p envelope appears as a 1:1 doublet, with one peak at 99.8 eV and another at 103 eV. A more careful peak fitting identifies that the envelope must contain at least two components, with one $2p_{1/2}-2p_{3/2}$ pair associated with silicon in metal silicides[10] and another pair associated with silicon in SiO_2 (Figs. 3a and c). The formation of silicon oxide on PtSi surface is also visible in the EDX mapping (2(e)). Given that Pt does not oxidize in air, we conjecture that the surface oxidation of PtSi produces a thin native oxide layer of SiO_2.

B. PtSi thin film electrical transport

The temperature-dependent electrical resistance of the PtSi thin film, $R(T)$, was measured from 300 K to 400 mK, clearly showing a sharp superconducting transition to zero resistance at 0.95 K (Fig. 4(a) and supplementary material Fig. S1), which is consistent with reported critical temperature (T_c) of PtSi.[15] In this study, we define T_c as the temperature that maximizes the derivative dR/dT, following a convention previously adopted for other superconducting materials.[23] The residual resistivity ratio (RRR) of our PtSi film, defined as ρ_{300K}/ρ_{1K}, is 2.25.

As a type II superconductor, PtSi is characterized by distinct phase transitions at two different applied magnetic fields.[15] Above the lower critical magnetic field (H_{c1}), the local suppression of the superconducting order parameter fosters the emergence of Abrikosov vortices, enabling the partial penetration of magnetic field. Above the upper critical field (H_{c2}), the superconducting order is destroyed entirely and the material reverts back to its normal state. The temperature dependent upper critical field is determined by measuring the electrical resistance in the temperature range of $0.41\ \mathrm{K} \leq T \leq 1.2\ \mathrm{K}$, with magnetic field $0\ \mathrm{mT} \leq \mu_0 H \leq 75\ \mathrm{mT}$ applied perpendicular to film surface (Fig. 4(b)). As T decreases from the critical temperature of PtSi (0.95 K), the superconducting order persists to incrementally higher magnetic fields (Fig. 4(b)). By applying the criterion R/R_n = 0.5, where R_n is the normal state resistance, we determined H_{c2} for each temperature, which is represented by the dashed black line in Fig. 4(b).

The upper critical field at 0 K, $H_{c2}(0)$, is determined according to the Werthamer-Helfand-Hohenberg model[24–27] in the dirty limit:

$$H_{c2}(0) = -\frac{\pi^2 T_c(0)}{8e^\gamma}\frac{dH_{c2}}{dT}\bigg|_{T=T_{c(0)}}, \tag{1}$$

where $T_c(0)$ is the critical temperature at zero field and $\gamma \approx$

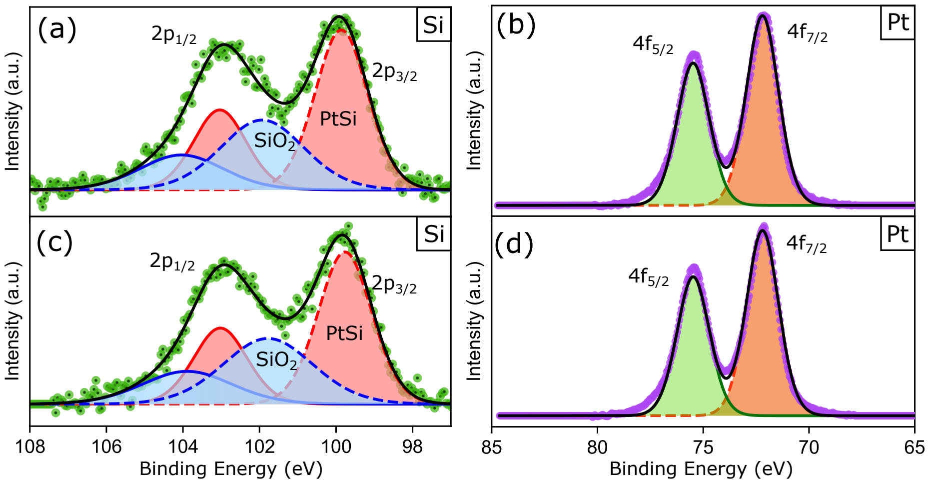

FIG. 3. XPS measurements across the PtSi thin film, for scans over (a, c) the Si 2p region and (b, d) the Pt 4f region. The spectra in (a) and (b) are collected near the edge of the 2-inch Si(100) wafer, while the (c) and (d) are scans collected near the wafer center. In each panel, the scatter plots show the experimental data, while the fitting envelopes are represented by solid black lines, which closely align with the measured spectrum.

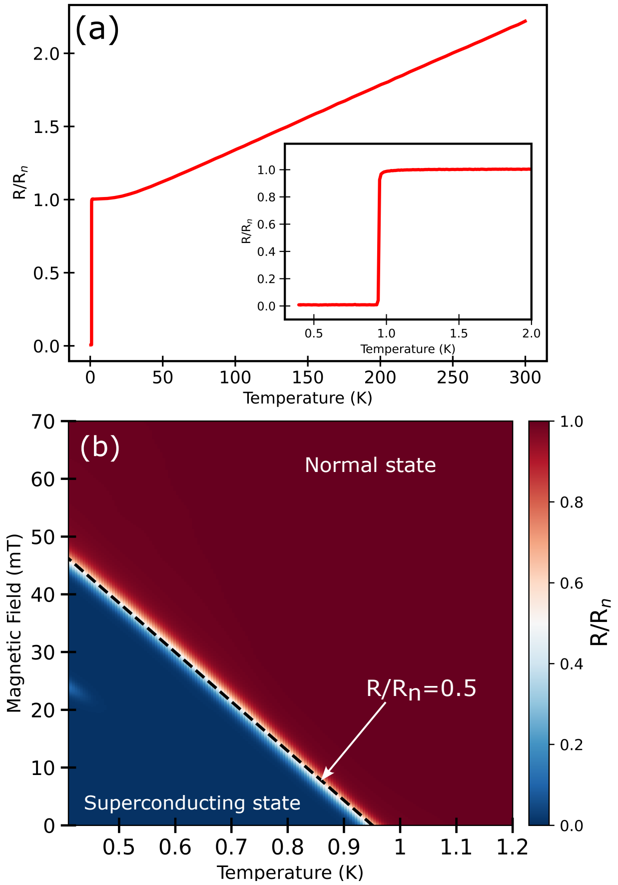

FIG. 4. (a) The temperature-dependent electrical resistance of a PtSi thin film from 300 K to 340 mK, showing superconducting transition at 0.95 K. Resistance values are normalized by the averaged resistance within the temperature range $1-2$ K. (*Inset*) Measured film resistance near the superconducting transition temperature. (b) Magnetic field phase diagram of superconducting PtSi. The narrow white region separates the normal state (red) and superconducting state (blue). A linear fit to $R/R_n = 0.5$ (dashed) finds $\mu_0 H_{c2}(0) = 56$ mT using Eq. (1).

0.5772 is Euler's constant. By performing a linear fit on the relationship between H_{c2} and T within the range of $0 \leq \mu_0 H_{c2} \leq 75$ mT, we derive the tangent term ($d\mu_0 H_{c2}/dT = -85.4$ mT/K) in Eq. (1) and determine that $\mu_0 H_{c2}(0) = 56$ mT.

$H_{c2}(0)$ is linked to the zero temperature Ginzburg-Landau (GL) coherence length, $\xi_{\rm GL}(0)$, through $\mu_0 H_{c2(0)} = \Phi_0/2\pi\xi_{\rm GL}^2(0)$, where $\Phi_0 = h/2e$ is the magnetic flux quantum,[28,29] which allows us to determine $\xi_{\rm GL}(0) = 76$ nm in these PtSi thin films. The relatively long coherence length, combined with the relatively high normal-state resistance of PtSi, positions it as a promising material for superconductor-constriction-superconductor (ScS) transmon, which can be fabricated in a single-step electron beam lithography process.[30] We can further estimate the Pippard coherence length using $\xi_0 = \hbar v_F/\pi\Delta(0)$, where v_F is the Fermi velocity and $\Delta(0)$ is the superconducting gap, $1.7k_BT_c$. The v_F is calculated as 0.33×10^6 $\mathrm{m\cdot s^{-1}}$, using the relation $v_F = \hbar(3\pi^2 n)^{1/3}/m_e$, with the carrier density $n = 7.9\times10^{20}$ $\mathrm{cm^{-3}}$ as determined by a density functional theory calculation.[31] The estimated Pippard coherence length, ξ_0, is around 460 nm. Through the dirty limit approximation $\xi_{\rm GL} \approx \sqrt{\xi_0 l}$, we estimate the electron mean free path l of 12 nm in these thin films.

We can estimate the Ginzburg-Landau parameter of our PtSi film, $\kappa = \lambda_{\rm eff}/\xi_{\rm GL}$, using these material constants. First, the zero temperature London penetration depth, $\lambda_L(0)$, is calculated to be 189 nm from $\lambda_L(0) = \sqrt{m_e/\mu_0 n e^2}$. From this, we estimate an effective penetration depth $\lambda_{\rm eff}$ of 326 nm, using $\lambda_{\rm eff}(0) = \lambda_L(0)\sqrt{1+\xi_0/l}$. We thus calculate $\kappa \approx 4.26$, as expected for a type-II superconductor. Because H_{c2} and H_{c1} are related through $H_{c2} = 2\kappa^2 H_{c1}$, we find $\mu_0 H_{c1} \approx 1.5$ mT in these thin films. Similarly, we may calculate the thermodynamic critical field as $\mu_0 H_c(0) = \mu_0 H_{c2}(0)/(\sqrt{2}\kappa) = 9.2$ mT.

C. PtSi microbridge device electrical transport

We pattern PtSi thin films into microbridge devices (Figs. 5 (a), (b)) by electron beam lithography and reactive ion etch-

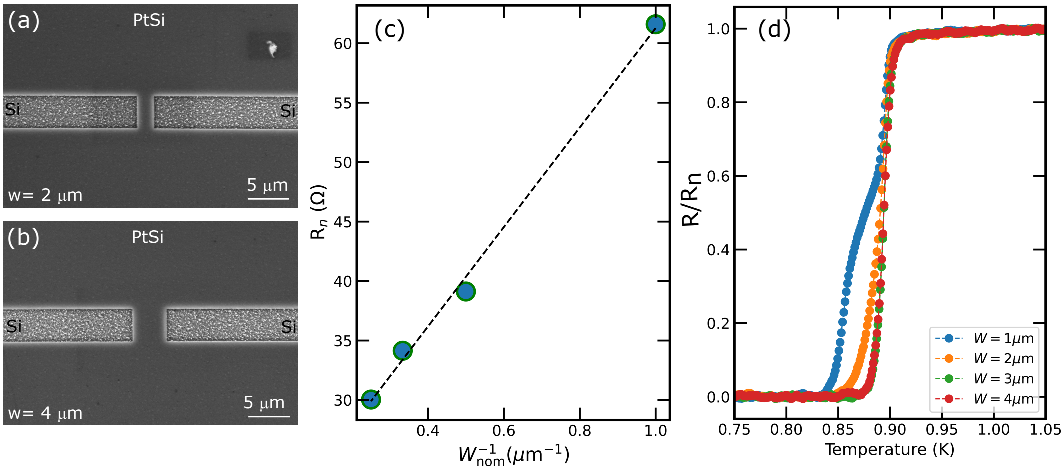

FIG. 5. SEM images on PtSi ScS type microbridge devices with (a) $w = 2$ μm and (b) $w = 4$ μm. (c) Normal state resistance as a function of inverse nominal width of the devices. The black dashed line represents the linear fit to the experimental data. The extracted normal state resistivity of PtSi from this linear fit is 26 $\mu\Omega$·cm. (d) The temperature dependence of the normalized resistance of PtSi devices.

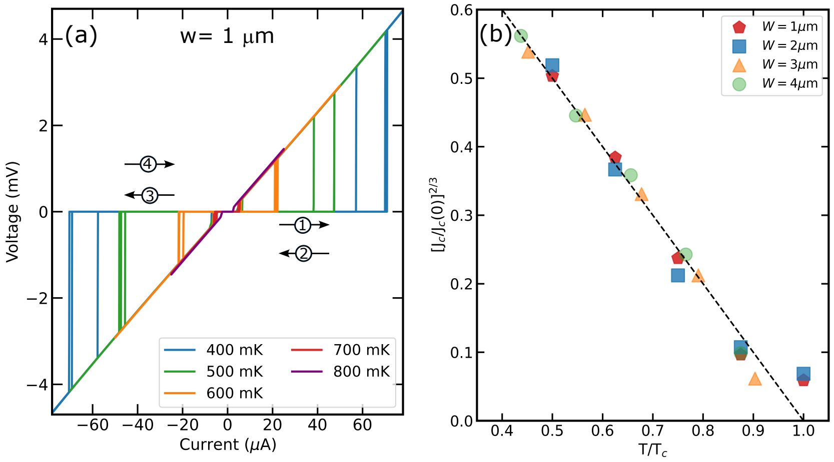

FIG. 6. (a) $V - I$ characteristics of a PtSi microbridge with $w = 1\mu m$, at different temperatures. The black arrows with numbers show the sequence of the current ramping directions. (b) The normalized critical current densities, $J_c/J_c(0)$, are plotted as a function of reduced temperature (T/T_c) for devices with different device channel widths. The dashed line corresponds to $[J_c/J_c(0)]^{2/3} = (1 - T/T_c)$.

ing (details in *Methods*). The microbridges have a length of 4 μm, with widths ranging from 1 to 4 μm. The device normal state resistance at 1 K (R_n) increases linearly with inverse nominal width (w_{nom}^{-1}) (Fig. 5(c)), as expected from the geometry, which allows us to extract a normal state PtSi resistivity of 26 $\mu\Omega$·cm from the slope. The 19 Ω residual resistance (y-intercept) in Fig. 5(b) reflects film resistance near the microbridge that is not compensated by the four-probe geometry. The PtSi resistivity value compares well with the previously reported value.[15] The temperature dependence of the normalized resistances, $R(T)/R_n$, are shown in Fig. 5(d). It appears that the T_c of wider microbridges ($w = 3$ and 4 μm) is close to the unpatterned thin film, but decreased slightly for narrower ones ($w = 1$ and 2 μm). In particular, a kink emerges at $R/R_n \approx 0.65$ for $w = 1$ μm. Note that the film resistance (~ 19 Ω) accounts for about one third of the total normal state resistance measured for the 1 μm microbridge, this suggests that the bridge remains in a mixed state when the bulk film completes superconducting transition. The behavior is consistent with thermal phase slip (TPS) that has larger impact to narrower microbridges. Calculation according to Little's model[28,32], however, finds that the superconducting condensation energy (ΔF_0) is much larger than thermal energy k_BT when the bulk value of H_c is used, while TPS is generally observed when ΔF_0 is smaller or comparable to $k_B T$. Nevertheless, this does not exclude TPS, as the reactive ion etching may have done enough damage to the edge, so that the local H_c and ΔF_0 become much smaller than their bulk values, with lower apparent T_c.[33] The temperature-dependent upper critical field of the microbridges, $H_{c2}(T)$, are similarly determined as the thin film, by measuring resistance R in the temperature range of $0.33\ \mathrm{K} \leq T \leq 1.0\ \mathrm{K}$, with magnetic field $-100\ \mathrm{mT} \leq \mu_0 H \leq 100\ \mathrm{mT}$. These microbridges show a similar $H_{c2}(T)$ as the PtSi thin film (supplementary material Fig. S2).

The microbridges of different widths showed generally similar voltage current($V-I$) characteristics and temperature dependence (supplementary material Fig. S3), as represented by the device with $w = 1\ \mu$m in Fig. 6(a). Below their T_c, the devices remain superconducting until the bias current reached a critical value, $I_c(T)$, at which point the device enters the normal state. Decreasing current in the normal state device transitions it back superconducting, at a retrapping current level I_r that is smaller than I_c. The black arrows with numbers in Fig. 6(a) show the sequence of the current ramping directions. For each temperature, $V-I$ measurements are repeated multiple times to obtain averaged I_c, at both positive and negative current bias. Fig. 6(b) shows the calculated J_c values from averaged I_c.

The superconducting-to-normal transition at I_c occurs when the kinetic energy of a Cooper pair exceeds its binding energy, resulting in de-pairing of the Cooper pair.[28] The de-pairing critical current density, $J_c(T)$, can be fit to the standard result of Ginzburg-Landau theory,[34,35]

$$J_c^{\mathrm{GL}}(T) = J_c^{\mathrm{GL}}(0)\left(1 - \frac{T}{T_c}\right)^{3/2}. \tag{2}$$

By averaging the fitting results for $w = 1-4\ \mu$m, we obtain $J_c^{\mathrm{GL}}(0) = (0.64 \pm 0.09)\ \mathrm{MA/cm^2}$ and $T_c = (0.84 \pm 0.06)$ K. As shown in Fig. 6(c), the scaling of $[J_c(T)/J_c(0)]^{2/3} \propto 1 - T/T_c$, as demanded by Eq. 2, is well preserved within the temperature range of study, for all 4 microbridge widths.

In some circumstances, de-pinning of Abrikosov vortices can also contribute to I_c, wherein the Lorentz force induced by the transport current surpasses the de-pinning force acting upon vortices in the superconductor, and initiating' movement.[36] The magnetic field generated by the transport current (I_T) at the edges of the PtSi bridges can be estimated using[37]

$$H_{edge} \approx \frac{I_T}{2\pi\sqrt{wt}}, \tag{3}$$

where t is the thickness of the thin film device. As shown in supplementary material Fig. S4, this field is only 0.16 mT, i.e., far below $\mu_0 H_{c1}$, and therefore the vortex depinning mechanism does not contribute significantly to I_c.

III. SUMMARY

In summary, we fabricated high quality, superconducting PtSi thin films and co-planar microbridge devices on silicon substrates, using magnetron sputtering, rapid thermal annealing, and reactive ion etching with a low-toxicity etchant. Low-temperature transport measurements, reveal a superconducting critical temperature of 0.95 K, which is suitable for superconducting quantum information applications hosted in a millikelvin dilution refrigerator, and an upper critical magnetic field of 56 mT. Our measurements confirm that PtSi is a type-II superconductor with a relatively long superconducting zero-temperature coherence length, $\xi_{\mathrm{GL}} = 76$ nm. This feature, combined with the relatively high normal state resistivity of PtSi, makes this material an attractive candidate for superconductor-constriction-superconductor (ScS) Josephson junctions and quantum phase-slip junctions. These advantages are further enhanced by the material's readiness for scalable patterning using CMOS-compatible processes.

IV. METHODS

A. Synthesis of PtSi thin films

PtSi thin films were synthesized over Si (100) wafers, by first depositing a thin layer of Pt (typically ~ 10 nm) on the Si wafer using magnetron sputtering (AJA Orion). Subsequently, the Pt-covered Si substrate went through rapid thermal processing (RTP) at 600°C for 10 minutes, in an inert atmosphere (4% H_2 in Ar), which converted the thin Pt layer into PtSi via reaction with the underlaying Si substrate. The native oxide on the Si wafer was a potential diffusion barrier and removed immediately before the Pt deposition, by immersing in a 10:1 buffered oxide etch (BOE) for 2 minutes. The Si wafer was further cleaned with deionized water and isopropanol, then dried under a stream of nitrogen gas and loaded into the Pt sputtering deposition chamber.

In this study, 2-inch undoped silicon <100> wafers from Virginia Semiconductor Inc were employed in the synthesis process and were carefully diced using laser dicing techniques before the device fabrication.

B. Material characterization

1. *Atomic force microscopy (AFM)*

The non-contact mode in the Park NX20 AFM was used to examine the surface topography of the PtSi thin film. The AFM images were processed using the XEI software from Park Systems Corporation.

2. *Grazing incident X-ray diffraction (GIXRD)*

X-ray diffraction (XRD) measurements of thin films employing traditional $\theta/2\theta$ scanning techniques typically receive weak signal from the thin films but intense signal from the substrates, and only capture reflection from crystalline planes that are parallel to the substrate surface. One of the approaches to evading the substrate signal while getting a strong signal from the thin film involves conducting a 2θ scan with a fixed grazing incidence angle. This method is commonly referred to as grazing incident X-ray diffraction (GIXRD).[38] The GIXRD patterns of the thin films were collected on a Rigaku SmartLab II X-ray diffractometer using Cu K_α radiation (λ = 1.5418 Å).

3. Scanning transmission electron microscopy (STEM)/ Focused ion beam (FIB)

The scanning transmission electron microscopy (STEM) and the energy-dispersive X-ray spectroscopy (EDX) studies were carried out on a JEOL ARM-200F, with the specimen prepared by the focused ion beam (FIB) lift-off technique using a dual beam SEM/ FIB microscope (FEI Helios).

4. X-ray photoelectron spectroscopy (XPS)

Surface chemistry of PtSi thin films was examined by X-ray photoelectron spectroscopy (XPS), using Al K_α radiation ($h\nu$ = 1486.6 eV) as the excitation source.

C. Device fabrication

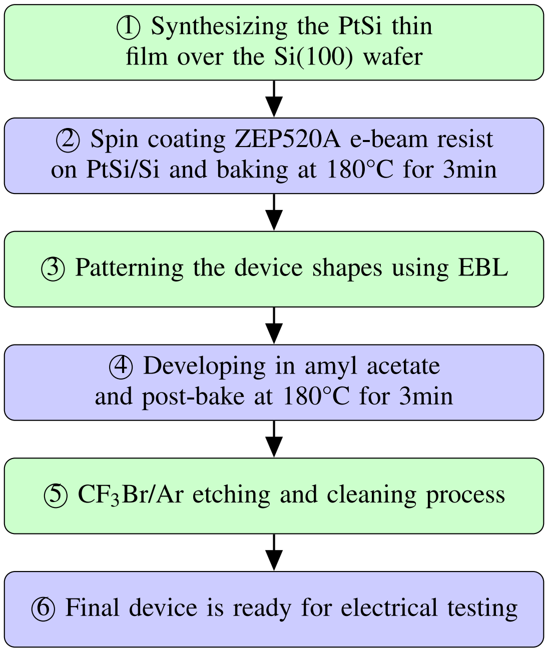

FIG. 7. Flow chart of the device fabrication process.

The flow chart in Fig. 7 illustrates the basic steps followed in device fabrication. The PtSi thin film was patterned into ScS weak link devices with a single step of electron beam lithography (EBL, JBX-6300FS), using a positive-tone, ZEP520A e-beam resist (ZEON). The PtSi wafer with ZEP520A was spun initially 500 rpm for 5 seconds and then 3000 rpm for 55 seconds to achieve a $\sim$ 420 nm thickness coverage on PtSi. Next, the e-beam resist coated PtSi wafer was baked at 180°C for 3 min and patterned using EBL. After developing in amyl acetate, the exposed areas of PtSi were etched away by reactive ion etching (RIE, March Plasma CS1701F), using a mixture of CF_3Br/Ar as the processing gas with the orifices of the mass flow controllers set at 8% and 6% respectively.[39] During the $\sim$4.5 minutes etching process, the plasma power was maintained at about 100 W, and the chamber's total pressure was stabilized close to 100 mT. The CF_3Br/Ar RIE would etch through exposed PtSi layer completely, with approximately 20 nm over-etching into the silicon substrate (supplementary material Fig. S5b).

In previous studies, RIE of PtSi thin films typically involved chlorine chemistry, e.g., in a gas mixture of Cl_2, CF_4, and Ar.[12] However, the use of Cl_2 in RIE processes requires strict safety measures and specialized equipment, due to its high toxicity. Therefore, our approach of using chlorine-free etching technique for PtSi is clearly advantageous. Additional details on CF_3Br/Ar etching characterization can be found in supplementary material Figs. S5 and S6. Finally, the e-beam resist mask was stripped overnight in a MICROPOSIT Remover 1165 bath at room temperature, followed by rinsing in 2-propanol and then dried under a stream of nitrogen gas.

D. Transport measurements on devices

Four terminal electrical transport measurements on PtSi devices were performed in a top-loading He-3 cryostat equipped with a superconducting magnet capable of 9 T. External magnetic fields were screened by a layer of metal shielding inside of the dewar that held the cryostat and magnet. The sample was sealed within a copper can at the bottom of the He-3 insert to shield out external signals. Noise was reduced in each measurement channel of the insert by low-temperature RC filters. Current biasing was provided by a low-noise DC current source and voltage was measured with a digital multimeter. Lumped LC low pass filters were used on each channel at room temperature. Resistance was determined by delta mode averaging with a bias current of 300 nA while slowly ($<$ 1 mK/s) sweeping temperature. It was found during the course of this work that the magnetic fields required for the measurements were not very large ($\leq$ 0.1 T). As such, the magnet's usual high current power supply was replaced with a high-precision DC current source to increase the resolution and precision of the applied magnetic fields. The four terminal electrical resistance measurements on the PtSi thin film sample were performed in a Quantum Design Dynacool 12 T Physical Property Measurement System (PPMS) equipped with a He-3 insert. For magnetic field-dependent measurements, the field was applied normal to the sample plane in both experimental setups.

SUPPLEMENTARY MATERIAL

Electrical transport characteristics of PtSi thin films and microbridges. Etching rate and roughness of CF_3Br/Ar RIE.

ACKNOWLEDGMENTS

This material is based upon work supported by the U.S. Department of Energy, Office of Science, National Quantum Information Science Research Centers, Co-design Center for Quantum Advantage (C^2QA) under contract number DE-SC0012704. This research used Materials Synthesis & Characterization, Electron Microscopy, and Proximal Probe facilities of the Center for Functional Nanomaterials (CFN), which is a U.S. Department of Energy Office of Science User Facility, at Brookhaven National Laboratory under Contract No. DE-SC0012704.

AUTHOR DECLARATION

Conflict of Interest: The authors have no conflicts to disclose.

AUTHOR CONTRIBUTIONS:

M.L. and C.T.B. conceptualized the project and supervised the project. T.N. and R.L. synthesized materials. A.K.R. helped with substrate preparation. T.N. fabricated the devices. K.K. and L.Z. conducted transmission electron microscopy experiments. A.T.B. and T.N. performed low-temperature transport measurements. C.Z. and X.T. conducted lab-based XPS studies. T.N., M.L., and C.T.B. drafted the manuscript. All authors participated in editing the manuscript.

DATA AVAILABILITY STATEMENT

Data generated and analyzed under this study is included in this article and available on reasonable request.

REFERENCES

[1] C. J. Richardson, V. Lordi, S. Misra, and J. Shabani, "Materials science for quantum information science and technology," MRS Bulletin **45**, 485–497 (2020).

[2] A. P. M. Place, L. V. H. Rodgers, P. Mundada, B. M. Smitham, M. Fitzpatrick, Z. Leng, A. Premkumar, J. Bryon, A. Vrajitoarea, S. Sussman, G. Cheng, T. Madhavan, H. K. Babla, X. H. Le, Y. Gang, B. Jäck, A. Gyenis, N. Yao, R. J. Cava, N. P. de Leon, and A. A. Houck, "New material platform for superconducting transmon qubits with coherence times exceeding 0.3 milliseconds," Nat. Commun. **12**, 3648–3655 (2021).

[3] A. Premkumar, C. Weiland, S. Hwang, B. Jäck, A. P. M. Place, I. Waluyo, A. Hunt, V. Bisogni, J. Pelliciari, A. Barbour, M. S. Miller, P. Russo, F. Camino, K. Kisslinger, X. Tong, M. S. Hybertsen, A. A. Houck, and I. Jarrige, "Microscopic relaxation channels in materials for superconducting qubits," Commun. Mater. **2**, 72 (2021).

[4] L. Grünhaupt, M. Spiecker, D. Gusenkova, N. Maleeva, S. T. Skacel, I. Takmakov, F. Valenti, P. Winkel, H. Rotzinger, W. Wernsdorfer, A. V. Ustinov, and I. M. Pop, "Granular aluminium as a superconducting material for high-impedance quantum circuits," Nat. Mater. **18**, 816–819 (2019).

[5] A. Schrauwen, J. Demeulemeester, D. Deduytsche, W. Devulder, C. Detavernier, C. Comrie, K. Temst, and A. Vantomme, "Ternary silicide formation from Ni-Pt, Ni-Pd and Pt-Pd alloys on Si(100): Nucleation and solid solubility of the monosilicides," Acta Mater. **130**, 19–27 (2017).

[6] C. Lavoie, F. d'Heurle, C. Detavernier, and C. Cabral, "Towards implementation of a nickel silicide process for cmos technologies," Microelectron. Eng. **70**, 144–157 (2003).

[7] W. S. W. Saitoh, S. Y. S. Yamagami, A. I. A. Itoh, and M. A. M. Asada, "35 nm metal gate p-type metal oxide semiconductor field-effect transistor with ptsi schottky source/drain on separation by implanted oxygen substrate," Jpn. J. Appl. Phys. **38**, L629 (1999).

[8] M. Hosseinifar, V. Ahmadi, and M. Ebnali-Heidari, "Si-Schottky photodetector based on metal stripe in slot-waveguide microring resonator," IEEE Photonics Technol. Lett. **28**, 1363–1366 (2016).

[9] S. P. Murarka, "Silicide thin films and their applications in microelectronics," Intermetallics **3**, 173–186 (1995).

[10] K. Idczak, S. Owczarek, and L. Markowski, "Platinum silicide formation on selected semiconductors surfaces via thermal annealing and intercalation," Appl. Surf. Sci. **572** (2022), https://doi.org/10.1016/j.apsusc.2021.151345.

[11] P. Szypryt, B. A. Mazin, G. Ulbricht, B. Bumble, S. R. Meeker, C. Bockstiegel, and A. B. Walter, "High quality factor platinum silicide microwave kinetic inductance detectors," Appl. Phys. Lett. **109**, 151102 (2016).

[12] P. Szypryt, S. R. Meeker, G. Coiffard, N. Fruitwala, B. Bumble, G. Ulbricht, A. B. Walter, M. Daal, C. Bockstiegel, G. Collura, N. Zobrist, I. Lipartito, and B. A. Mazin, "Large-format platinum silicide microwave kinetic inductance detectors for optical to near-IR astronomy," Opt. Express **25**, 25894–25909 (2017).

[13] M. M. Islam, S. Alam, M. S. Hossain, K. Roy, and A. Aziz, "A review of cryogenic neuromorphic hardware," J. Appl. Phys. **133** (2023), 10.1063/5.0133515.

[14] T. I. Baturina, D. Horsell, D. Islamov, I. Drebushchak, Y. Tsaplin, A. Babenko, Z. Kvon, A. Savchenko, and A. Plotnikov, "Josephson junction arrays on the basis of superconducting ptsi films," Physica B **329-333**, 1496–1497 (2003).

[15] K. Oto, S. Takaoka, K. Murase, and S. Ishida, "Superconductivity in PtSi ultrathin films," J. Appl. Phys. **76**, 5339–5342 (1994).

[16] A. Wawro, S. Suto, and A. Kasuya, "STM studies of PtSi formation on si(111) by solid state epitaxy," Phys. Rev. B **72**, 205302 (2005).

[17] A. A. Naem, "Platinum silicide formation using rapid thermal processing," J. Appl. Phys. **64**, 4161–4167 (1988).

[18] N. Ye, J. P. Feser, S. Sadasivam, T. S. Fisher, T. Wang, C. Ni, and A. Janotti, "Thermal transport across metal silicide-silicon interfaces: An experimental comparison between epitaxial and nonepitaxial interfaces," Phys. Rev. B **95**, 085430 (2017).

[19] R. Kraehnert, E. Ortel, B. Paul, B. Eckhardt, M. Kanis, R. Liu, and A. Antoniou, "Electrochemically dealloyed platinum with hierarchical pore structure as highly active catalytic coating," Catal. Sci. Technol. **5**, 206–216 (2015).

[20] L. Ley, Y. Wang, V. Van, S. Fisson, D. Souche, G. Vuye, and J. Rivory, "Initial stages in the formation of PtSi on Si(111) as followed by photoemission and spectroscopic ellipsometry," Thin Solid Films **270**, 561–566 (1995).

[21] H. Zhang, G. She, J. Xu, S. Li, Y. Liu, J. Luo, and W. Shi, "Electrochemical surface reconstructed $Pt_{x(x=2,3)}Si$/PtSi/p-Si photocathodes for achieving high efficiency in photoelectrochemical H_2 generation," J. Mater. Chem. A **10**, 4952–4959 (2022).

[22] F. Streller, G. E. Wabiszewski, F. Mangolini, G. Feng, and R. W. Carpick, "Tunable, source-controlled formation of platinum silicides and nanogaps from thin precursor films," Adv. Mater. Interfaces **1**, 1300120 (2014).

[23] S. Yadav, V. Kaushik, M. P. Saravanan, R. P. Aloysius, V. Ganesan, and S. Sahoo, "A robust nitridation technique for fabrication of disordered superconducting tin thin films featuring phase slip events," Sci. Rep. **11**, 7888 (2021).

[24] W. Zhang, A. T. Bollinger, R. Li, K. Kisslinger, X. Tong, M. Liu, and C. T. Black, "Thin-film synthesis of superconductor-on-insulator A15 vanadium silicide," Sci. Rep. **11**, 2045–2322 (2021).

[25] N. R. Werthamer, E. Helfand, and P. C. Hohenberg, "Temperature and purity dependence of the superconducting critical field, H_{c2}. iii. electron spin and spin-orbit effects," Phys. Rev. **147**, 295–302 (1966).

[26] Z. Ryżyńska, J. R. Chamorro, T. M. McQueen, P. Wiśniewski, D. Kaczorowski, W. Xie, R. J. Cava, T. Klimczuk, and M. J. Winiarski, "Rual6—an endohedral aluminide superconductor," Chem. Mater. **32**, 3805–3812 (2020).

[27] F. Marsili, M. J. Stevens, A. Kozorezov, V. B. Verma, C. Lambert, J. A. Stern, R. D. Horansky, S. Dyer, S. Duff, D. P. Pappas, A. E. Lita, M. D. Shaw, R. P. Mirin, and S. W. Nam, "Hotspot relaxation dynamics in a current-carrying superconductor," Phys. Rev. B **93**, 094518 (2016).

[28] M. Tinkham, Introduction to superconductivity (Courier Corporation, 2004).

[29] G. Deutscher, O. Entin-Wohlman, and Y. Shapira, "Upper critical fields in granular superconductors," Phys. Rev. B **22**, 4264–4270 (1980).

[30] M. Liu and C. T. Black, "Performance analysis of superconductor-constriction-superconductor transmon qubits," Phys. Rev. A **110**, 012427 (2024).

[31] A. Slepko and A. A. Demkov, "Band engineering in silicide alloys," Phys. Rev. B **85**, 035311 (2012).

[32] W. A. Little, "Decay of persistent currents in small superconductors," Phys. Rev. **156**, 396–403 (1967).

[33] S. Ishida, K. Murase, K. Gamo, and S. Namba, "Quantum transport in ptsi thin films and narrow wires," J. Phys. Soc. Jpn. **64**, 858–871 (1995).

[34] W. J. Skocpol, M. R. Beasley, and M. Tinkham, "Self-heating hotspots in superconducting thin-film microbridges," J. Appl. Phys. **45**, 4054–4066 (2003).

[35] K. Ilin, D. Rall, M. Siegel, A. Engel, A. Schilling, A. Semenov, and H.-W. Huebers, "Influence of thickness, width and temperature on critical current density of nb thin film structures," Physica C **470**, 953–956 (2010).

[36] D. Dew-Hughes, "The critical current of superconductors: an historical review," Low Temp. Phys. **27**, 713–722 (2001).

[37] E. Zeldov, J. R. Clem, M. McElfresh, and M. Darwin, "Magnetization and transport currents in thin superconducting films," Phys. Rev. B **49**, 9802–9822 (1994).

[38] K. V. Chizh, V. P. Dubkov, V. M. Senkov, I. V. Pirshin, L. V. Arapkina, S. A. Mironov, A. S. Orekhov, and V. A. Yuryev, "Low-temperature formation of platinum silicides on polycrystalline silicon," J. Alloys Compd. **843**, 155908 (2020).

[39] D. L. Flamm, P. L. Cowan, and J. A. Golovchenko, "Etching and film formation in CF_3Br plasmas: some qualitative observations and their general implications," J. Vac. Sci. Technol. **17**, 1341–1347 (1980).